



Silver-Doped Cadmium Oxide Nanoparticles Synthesized by Laser Ablation in Liquid for NO₂ and H₂S Gases' Detection

Zainab A. Abbas¹ · Khawla S. Khashan¹ · Zainab T. Hussain²

Received: 3 February 2023 / Accepted: 28 February 2023 / Published online: 10 March 2023
© The Author(s), under exclusive licence to Springer Science+Business Media, LLC, part of Springer Nature 2023

Abstract

Pulsed laser ablation in liquid technique was used to prepare pure and doped CdO NPs with varied Ag concentrations. The prepared nanoparticles were characterized using Fourier-transform infrared spectroscopy (FTIR), X-ray diffraction (XRD), UV–vis spectroscopy, Field-emission scanning electron microscopy (FESEM) with energy dispersive spectroscopy (EDS), and atomic force microscopy. The FTIR and XRD data confirm the construction of CdO NPs doped with Ag. The morphology of pure CdO NPs was found to be agglomerated in bundles that resemble tangled nanowires, which changed to nanorods and interconnecting web architectures as Ag concentration increased. The absorption of these nanoparticles varied with Ag doping concentrations. Additionally, the gas-sensing properties of the pure and doped CdO sensor were investigated. The gas-sensing response of the composite nanoparticles' sensor to NO₂ was 46, which was 1.8 times larger than the response of the pure CdO NP sensor (24.9). Thus, oxidizing gas (NO₂) was found to be less sensitive to Ag-doped CdO nanocomposite sensors than reducing gas (H₂S).

Keywords CdO NPs · Ag-doped CdO · Gas sensor · PLAL · Gas sensor · Gas sensor

Introduction

Nanotechnology is a new and fast-arising field that involves the fabrication, treatment, and application of structures, systems, and devices by controlling size and shape at the nanometer scale. Nanoparticles have attracted significant research interest in recent years due to their specific chemical, physical, and surface properties associated with their size, which can vary from those of individual atoms or bulk materials [1–4]. One of the several applications for materials with nanostructures is gas sensor, and numerous studies have been conducted on metal oxide semiconducting nanostructure-based gas sensors. It has been proven that decreasing the size of the crystals results in a high surface-to-volume ratio, which considerably improves sensor performance. This is because metal oxide grains that are nearly depleted in carriers display larger conductance changes when exposed to target gases due to more carriers being activated from their

trapped states to the conduction band [5–8]. Among metal oxide semiconductor materials, CdO nanoparticles are particularly interesting due to their outstanding characteristics, such as narrow bandgap, high optical transparency in the visible region, simple crystal structures, high carrier mobilities, and high electrical conductivity [9–13]. These characteristics make them applicable in photoelectric devices, liquid crystal displays, semiconductor lasers, and gas sensors. However, CdO has been further improved in terms of gas-sensing ability by doping it with other metals such as Pt, Al, In, Zn, Au, Ag, and Pd [14–19]. Silver, in particular, has been used in modification processes due to its low cost, ease of oxidation, strong electrical conductivity with quick electron transfer, ease of preparation, and ability to drastically alter the bandgap in the structure; it has been used in modification processes [20–22]. Various methods, including sol–gel [17], spray pyrolysis [18], co-precipitation [13], and hydrothermal [8], have been used to create pure and doped CdO nanoparticles. Among them, pulsed laser ablation in liquid is the most straightforward, economical, exact, and environmentally friendly technology used to create nanomaterials of various sizes and shapes by adjusting the laser ablation settings and types of liquid media [4, 23–28]. In this study, we present the fabrication of gas sensors based on Ag-doped CdO nanoparticles produced in liquid by pulsed

✉ Khawla S. Khashan
khawla_salah@yahoo.com

¹ Applied Science Department, University of Technology, Baghdad, Iraq

² Ministry of Science and Technology, Baghdad, Iraq

laser ablation. We also describe the structural, morphological, and optical characteristics of pure and Ag-doped CdO nanoparticles and investigate their gas-sensing capabilities.

Experimental Work

The following steps were used to create samples of both pure and Ag-doped CdO NPs: to create pure CdO NPs, a cadmium target (Cd, 99.99%, Sigma-Aldrich, Saint Louis, USA) was placed at the bottom of a small container filled with 3 ml of deionized water (DIW). The Q-switch Nd:YAG laser source (1064 nm, 1 Hz, 9 ns) was used for the ablation process, producing 300 mJ of laser energy over 300 pulses. To create an Ag-doped CdO nanocomposite, a silver target (Ag, 99.9%) was added to a solution containing CdO NPs, and the mixture was ablated using a constant laser energy of 300 mJ and various pulse counts (20, 30, 40, and 50).

Different experimental measures were used to characterize the resulting nanostructure materials. Fourier-transform infrared (FTIR) spectra were captured in the 4000 to 400 cm^{-1} regions using a Shimadzu (8000 Series, Shimadzu, IRAffinity-1, Japan) spectrometer. X-ray analyses were performed using a PW 1730 diffractometer and Cu K radiation (30 kV X 10 mA). The optical absorbance characteristics of the NPs were evaluated using a UV–visible double-beam spectrophotometer (Schimatzu, 1800). The morphology was examined using field-emission scanning electron microscopy (FESEM, Czech Republic, Tescan, Mira III).

The sensing device was fabricated by drop-casting a nanocomposite solution onto a silicon wafer. The resistance

in air (R_a) and the resistance in test gases H_2S and NO_2 (R_g) were measured to calculate the sensitivity (S). The time required to reach 90% of the response signal was known as the response time, or T_{res} . The recovery times, T_{rec} , were measured in terms of the time required to restore 90% of the initial baseline signal. The experiments were conducted using 3 V bias voltages, several operating temperatures, and a 25-ppm gas concentration.

Result and Discussion

The FTIR spectra of pure and Ag-doped CdO NPs with various doping ratios (0.33%, 0.60%, and 0.71%) are presented in Fig. 1. The wide band at approximately 3400 cm^{-1} for all samples is caused by the O–H stretching bands of the hydroxyl assembly of CdO NPs and the water molecules chemically associated with them. The peaks at 1380 cm^{-1} are associated with the wagging band of the pure sample, while new peaks arise at 1130 cm^{-1} in doped samples, designated as a metal–oxygen bond on Ag–CdO NP samples, confirming the successful doping of Ag in CdO NPs. The peaks at 660 cm^{-1} in all samples are due to the Cd–O stretching vibration [3, 11, 29].

Figure 2 shows the XRD pattern of pure and Ag-doped CdO NPs at different concentrations. The cubic CdO phase (311), (111), (200), (422), and (440) orientations at 2θ of 30.55°, 36.5°, 38.5°, 43.95°, and 50.05°, respectively, are observed in the pure CdO NPs (JCPDS: 05–0640), and additionally peak with an index of (111) planes appeared at 2θ of 33.25° for the sample doped with 0.71% Ag [22]. The cubic phase of CdO can be observed in the diffraction peaks

Fig. 1 FTIR spectra of pure and Ag-doped CdO NPs

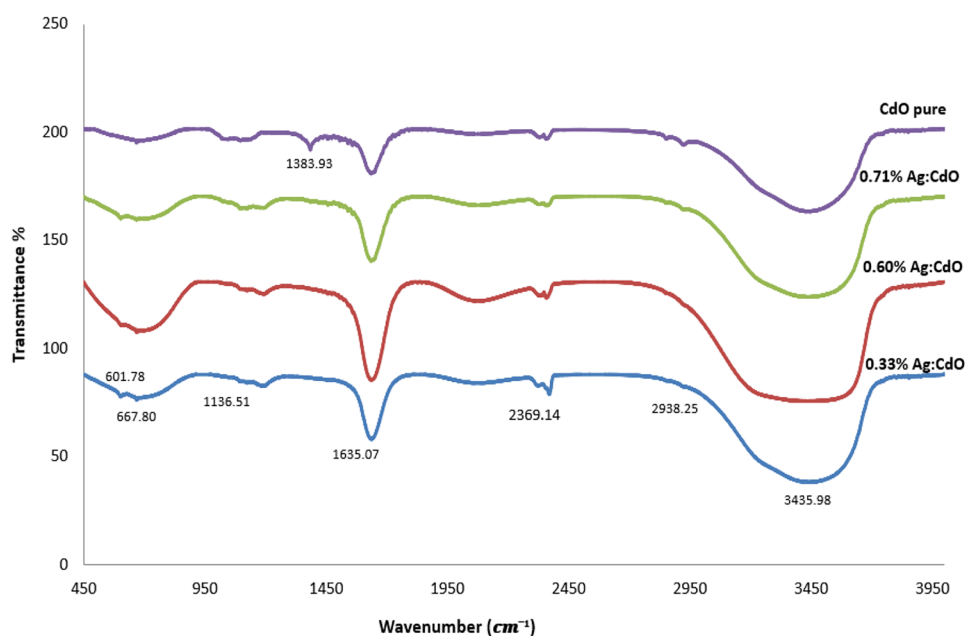
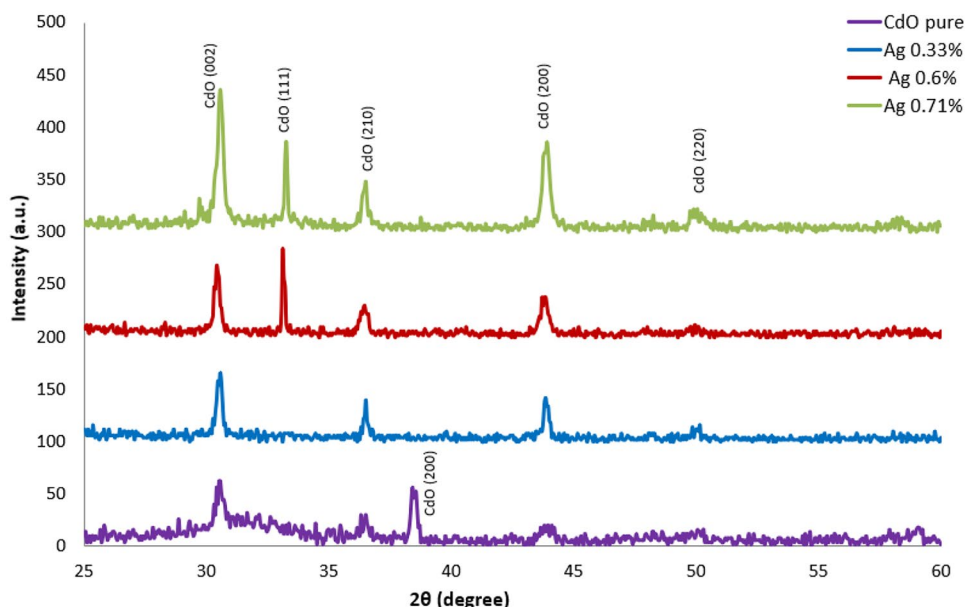


Fig. 2 XRD pattern of pure and Ag-doped CdO NPs

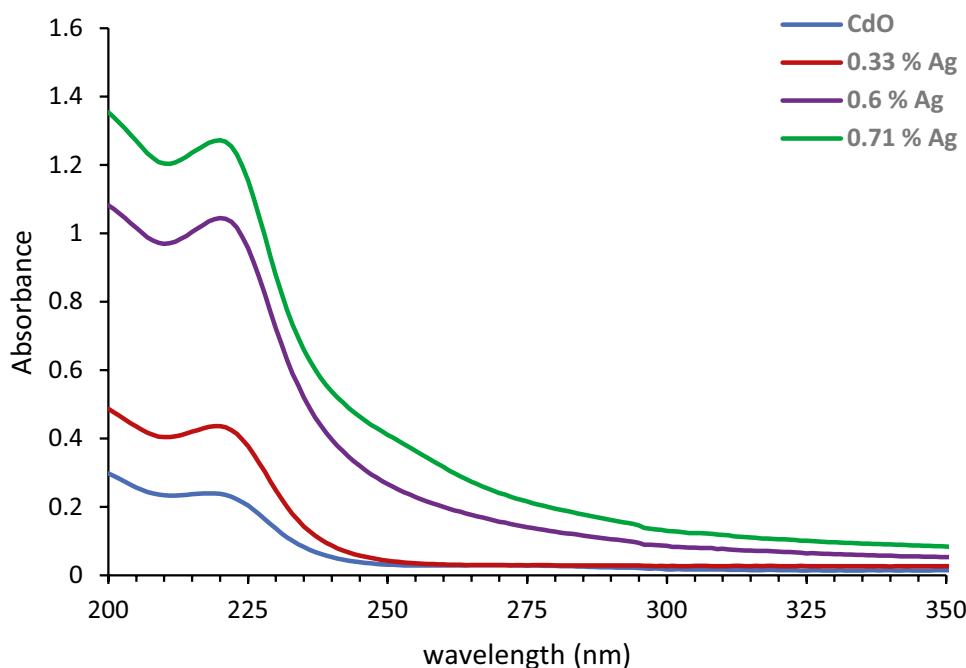


of both pure and Ag-doped samples, and their intensities increase as the doping concentration rises, and no additional impurity peaks are observed.

Figure 3 shows the optical absorbance of pure and Ag-doped CdO NPs with various doping ratios (0.33%, 0.60%, and 0.71%). The absorbance was measured as a function of wavelength, and it is evident that the intensity of the absorbance increased with increasing amounts of Ag doping [30]. This is due to the formation of increased levels of impurities inside the energy gap, which increased the absorption, with a peak at around 220 nm that slightly shifted to red wavelength

due to the $n-\pi^*$ transition of electrons. The optical band gap E_g can be calculated by Tauc's formula: $ah\nu = A(h\nu - E_g)^n$, where α is the absorption coefficient, h is Planck's constant, ν is the photon frequency, A is constant, and n is the transition constant [20]. Figure 4 shows the optical band gaps, which were found to be 2.9 eV for pure CdO and between 1.6 and 3 eV for Ag-doped CdO. The presence of two optical band gaps may be due to the formation of nanoparticles with different sizes and shapes [31]. Furthermore, the variations in the optical band gap in nanomaterials can be explained based on the quantum size effect [2]. Thus, the increase in

Fig. 3 absorbance spectra of CdO NPs and doped with Ag at different ratios



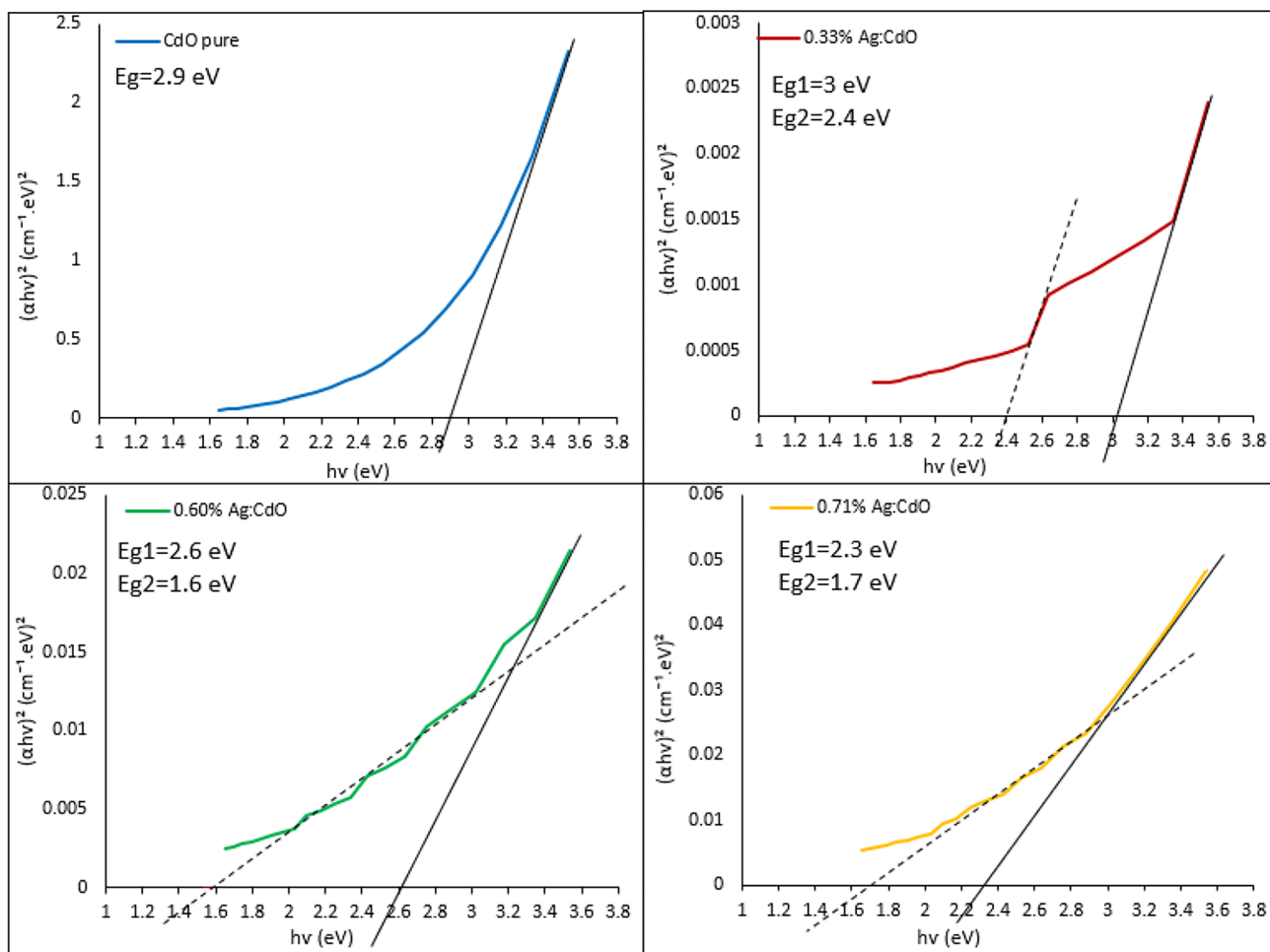


Fig. 4 The optical band gaps of pure and Ag-doped CdO NPs

sensitivity with a decrease in particle size can be attributed to the surface-to-volume ratio. The smaller the diameter, the higher the surface-to-volume ratio, and therefore, the greater the adsorption of gas [32].

A FESEM micrograph of pure CdO NPs and Ag-doped CdO NPs with varying doping concentrations is shown in Fig. 5. In Fig. 5a, pure CdO NPs are found agglomerated in bundles that resemble tangled nanowires due to the van der Waals force that occurs between the wires [20]. Figure 5b shows the FESEM morphology of 0.6% Ag-doped CdO NPs, where larger nanorod aggregates of CdO NPs and erratic Ag particles with a size shift from (21.7 nm) to (52.7 nm) are observed. The FESEM morphology of 0.71% Ag-doped CdO NPs is shown in Fig. 5c, where additional nanorods can be seen interacting and interconnecting as web architectures of CdO NPs and irregular Ag particles with size changes from (18.55 nm) to (66.89 nm); therefore, sensitivity increases as particle size decreases [33]. The presence of

Cd, O, and Ag elements was verified by the EDS elemental composition of pure CdO NPs and Ag-doped CdO NPs (Fig. 6). While pollution may be the cause of the presence of the C element, it is also evident that the intensity of the elements significantly changes when the doping ratio varies.

Pure and Ag-doped CdO nanoparticles were imaged using an AFM across an area of $(1.0 \times 1.0) \mu\text{m}^2$ in Fig. 7. These images demonstrate that the Ag doping concentration had a significant impact on the surface morphologies of the films. It is evident that as the Ag doping level increased, the films' surface roughness decreased. The sensing response of pure and doped CdO nanoparticles is enhanced when the surface roughness is reduced owing to improved adsorption and interaction between the gas molecules and the sensing material. Additionally, a smoother surface may reduce the scattering of incident light and increase the transmission of light through the sensing material, leading to improved signal-to-noise ratios in optical sensing applications [34].

Fig. 5 FESEM micrograph of pure and Ag-doped CdO NPs: **a** pure CdO, **b** 0.6%, and **c** 0.71%

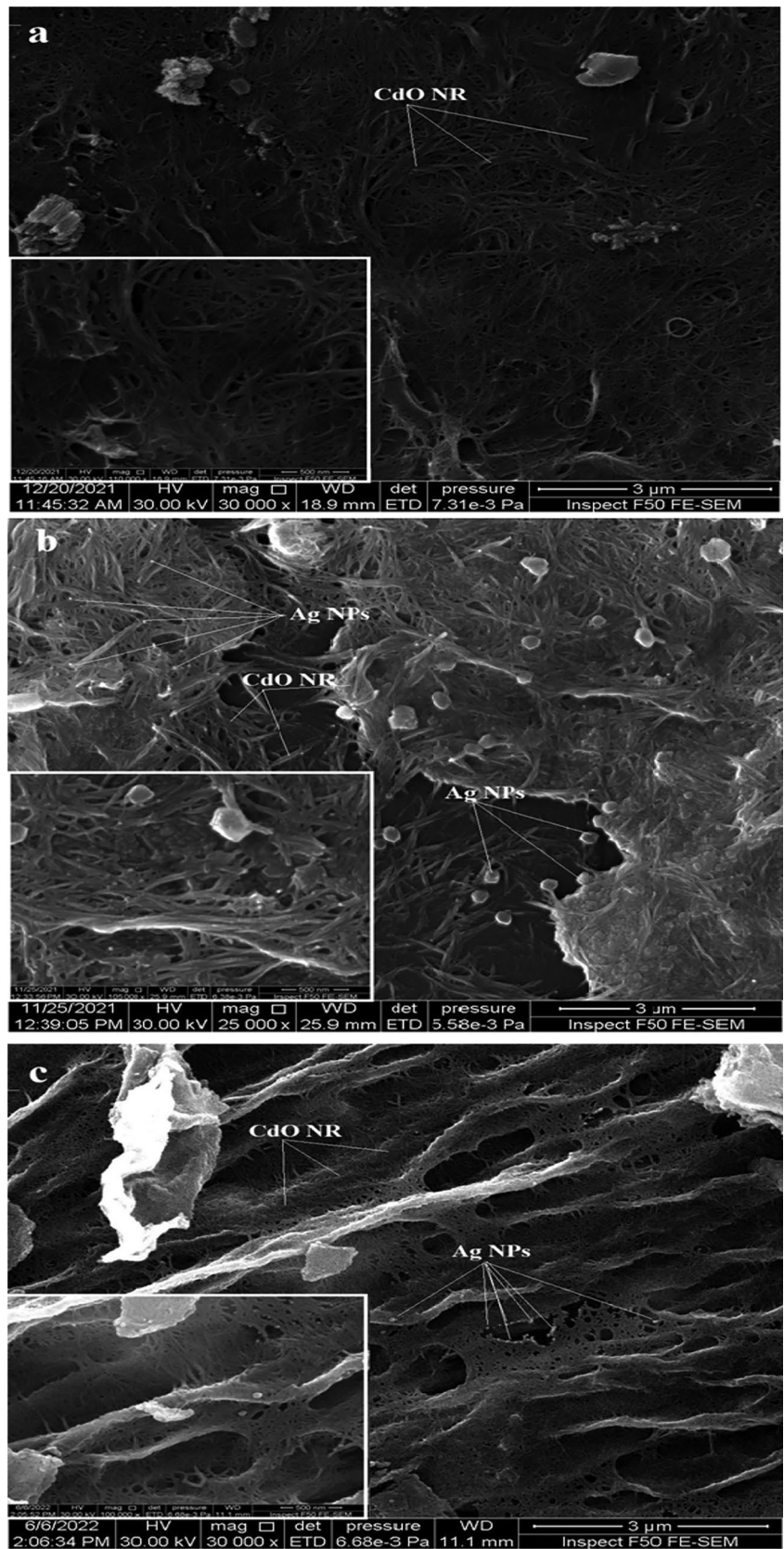
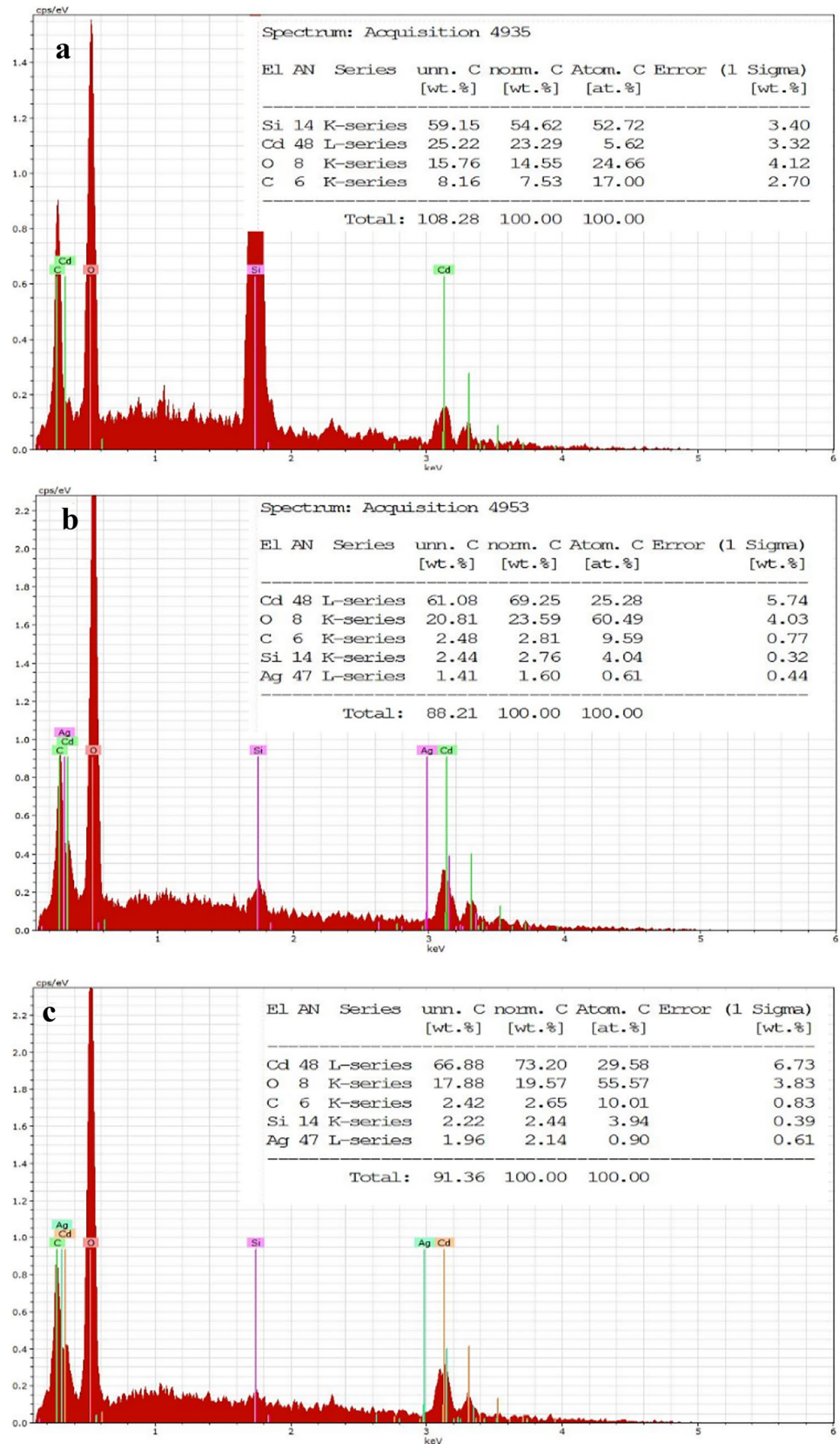


Fig. 6 EDS spectrum of pure and Ag-doped CdO NPs at various doping ratios: **a** pure CdO NPs, **b** 0.60%, and **c** 0.71%



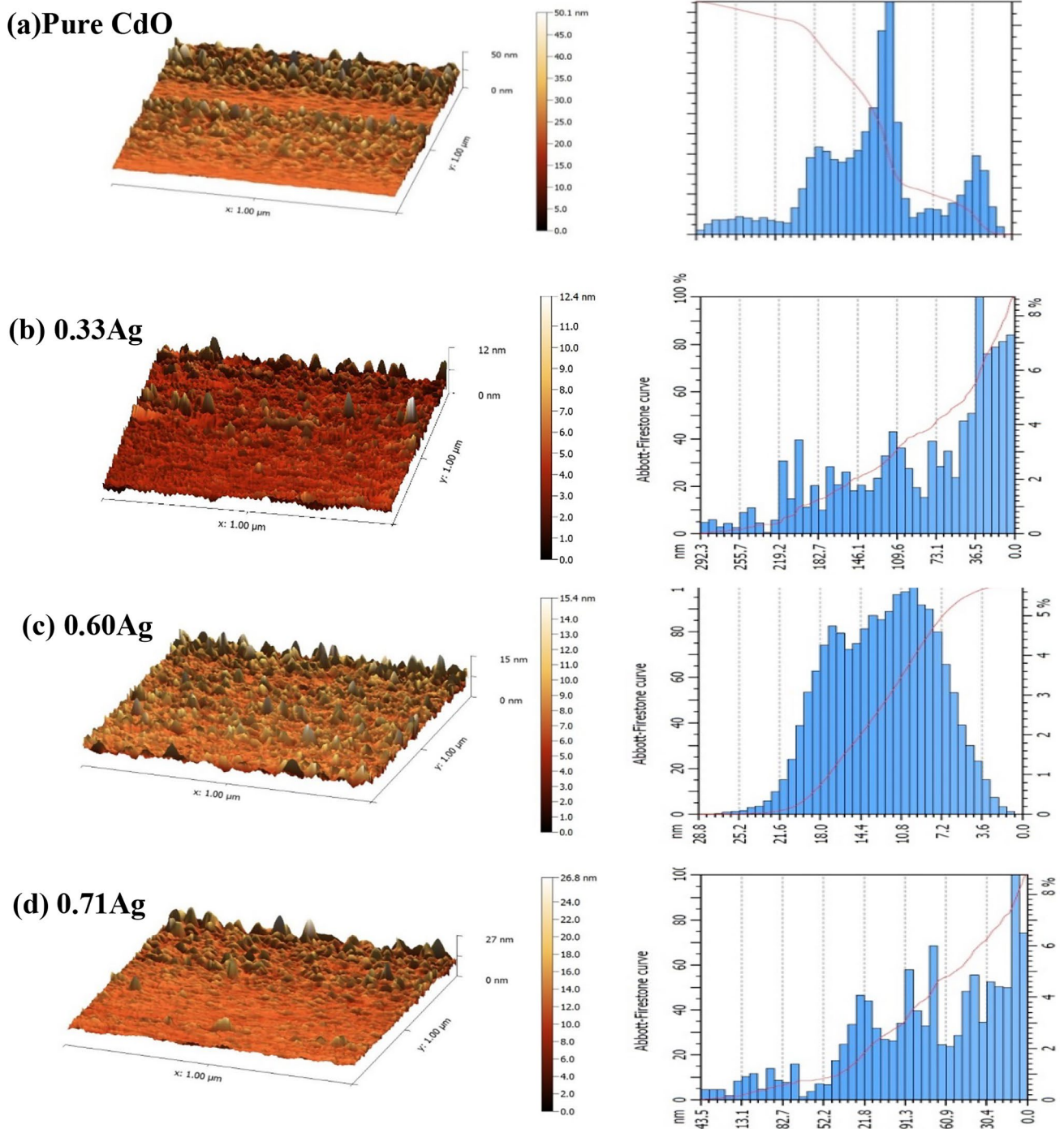


Fig. 7 AFM images of pure and Ag-doped CdO NPs

Figures 8 and 9 illustrate the sensitivity for pure CdO NPs and doping with various concentrations of Ag at H₂S and NO₂ gases as a function of operating temperature in the range of 100–300 °C. The testing for gas sensitivity started at 100 °C and went up to 300 °C in 100 °C increments. The

data show that the sensitivity increases with increasing operating temperature. The statistics show that the sensitivity of all samples increases with increasing operating temperature. This is connected to a rise in the rate of surface reactivity of the target gas. The relationship between sensitivity

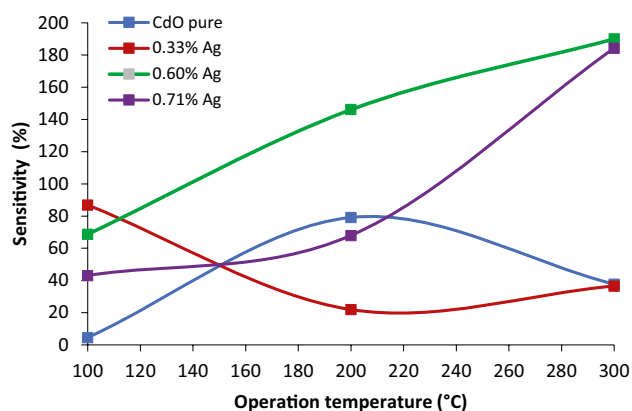


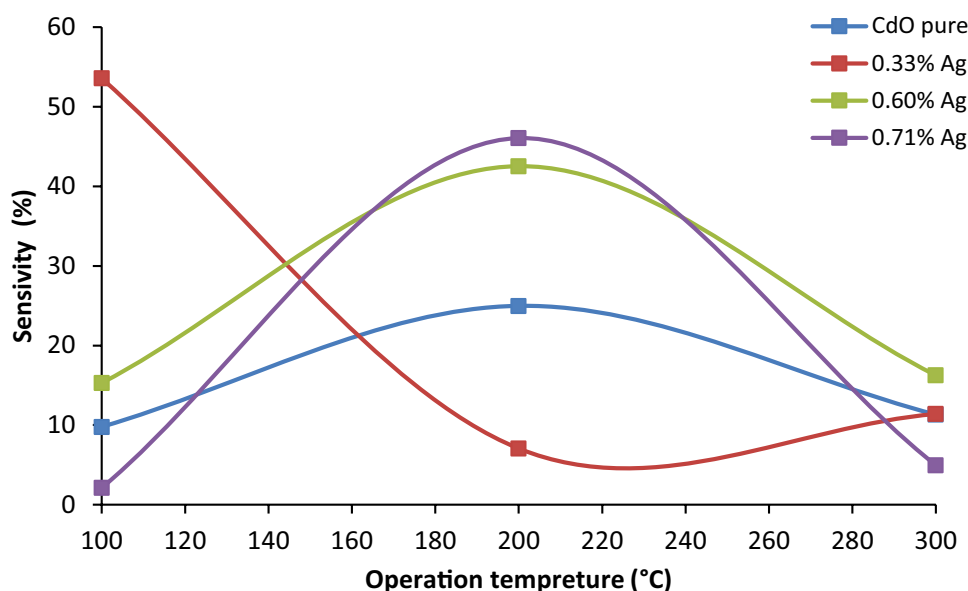
Fig. 8 Sensitivity of pure and Ag-doped CdO NPs to H₂S gas at various doping ratios

and temperature for semiconductor metal oxide gas sensors resembles a volcano because maximal peak values are seen at specific temperatures known as the optimum temperature and then decline as the temperature rises [35, 36]. According to Fig. 8, pure CdO NPs are substantially less sensitive to H₂S than CdO NPs that have been doped with Ag. The created oxygen vacancies can act as a trapping site for O₂ molecules when a semiconductor is exposed to air, providing electrons as a result of their local electronic charge, and the free O₂ molecules transform into peroxide or superoxide ions. The H₂S sensor also has an impressive detection range of around S = 190 at 300 °C. The much lower O₂ dissociation

adsorption energy on the Ag-doped surface compared to the undoped CdO surface further shows that Ag is a far better oxygen dissociation catalyst than CdO. Almost 5.1 times larger than the reaction of the pure CdO NP sensor, the composite NP sensor's response to H₂S is (190) (37.7). As shown in Fig. 9, the great sensitivity for NO₂ detection was demonstrated at 200 °C for a sample doped with 0.71% Ag. Additionally, Ag-doped CdO NWs have higher sensitivity than pure CdO NWs. This study demonstrates how silver doping and silver ion precipitation can increase sensitivity. Moreover, the response of the composite NP sensor to NO₂ (46) is 1.8 times higher than that of the pure CdO NP sensor (24.9). This result is consistent with reference [37] and shows that reducing gas (H₂S) is more sensitive to Ag/CdO composite NP sensors than oxidizing gas (NO₂).

For NO₂ (Fig. 10a) and H₂S (Fig. 10b) gases at various operating temperatures, Fig. 10 illustrates the relationship between the response time and the recovery time for pure and Ag-doped CdO NPs. According to Fig. 10a, samples containing 0.6% of Ag have a short response-recovery time, which is likely due to the catalytic activity of metallic Ag [38]. Additionally, the 0.60 Ag-CdO sensor in Fig. 10b has the fastest reaction time. Ag may effectively speed up the measurement of the gas and the adsorption of oxygen ions. Ag is easily transformed into Ag₂O in the presence of air, and CdO NPs lose electrons, resulting in a deeper electron depletion area. CdO/Ag effectively lowers the optimal operating temperature, increases the gas response value, and accelerates response and recovery times [39].

Fig. 9 Sensitivity of pure and Ag-doped CdO NPs to NO₂ gas at different doping ratios



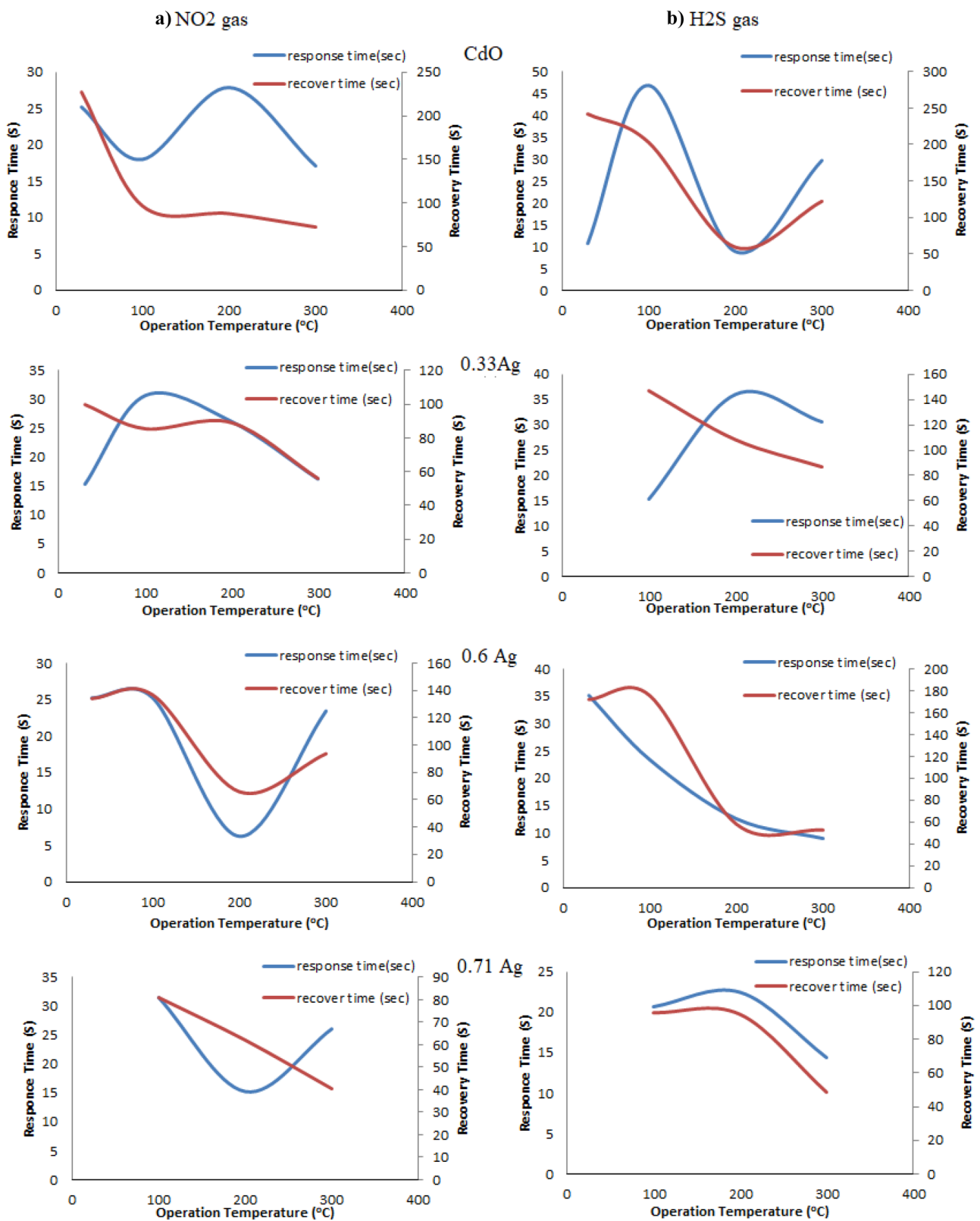


Fig. 10 Response and recovery time to NO₂ (a) and H₂S (b) gases for pure and Ag-doped CdO NPs

Conclusions

In a green and ecologically friendly process, pure and Ag-doped CdO nanoparticles are created using Nd:YAG pulsed laser ablation in liquid. The presence of CdO nanoparticles in Ag is confirmed by the FTIR results, while XRD analysis reveals a crystalline material with a cubic structure. Additionally, FESEM analysis shows that the synthesized nanoparticles form nanorod-shaped aggregates, and EDS analysis confirms the presence of Cd, O, and Ag. The optical absorbance and surface morphology of CdO NPs are affected by the Ag concentration, and the doped structure displays high sensitivity and a quick response/recovery time. As a result, this method represents an inexpensive and efficient way to create metal oxide nanostructures without the need for post-synthesis heating.

Acknowledgements The University of Technology in Baghdad, Iraq, provided assistance, which the authors are grateful for.

Author Contribution Conceptualization, K. S. K. and Z. T. H.; methodology, K. S. K., Z. T. H., and Z. A. A.; formal analysis, K. S. K., Z. T. H., and Z. A. A.; investigation, K. S. K., Z. T. H., and Z. A. A.; data curation, K. S. K., Z. T. H., and Z. A. A.; writing—original draft preparation, K. S. K., Z. T. H., and Z. A. A.; supervision, K. S. K. and Z. T. H.; project administration, K. S. K.; all authors have read and agreed to the published version of the manuscript.

Availability of Data and Materials The data used to support the findings of this study are included in the article.

Declarations

Ethics Approval Not applicable.

Competing Interests The authors declare no competing interests.

References

1. Radi PA, Brito-Madurro AG, Madurro JM, Dantas NO (2006) Characterization and properties of CdO nanocrystals incorporated in polyacrylamide. *Braz J Phys* 36:412–414
2. Ismail RA, Khashan KS, Alwan AM (2017) Study of the effect of incorporation of CdS nanoparticles on the porous silicon photodetector. *SILICON* 9(3):321–326
3. Sivakumar S, Venkatesan A, Soundhirarajan P, Khatiwada CP (2015) Synthesis, characterizations and anti-bacterial activities of pure and Ag doped CdO nanoparticles by chemical precipitation method. *Spectrochim Acta Part A Mol Biomol Spectrosc* 136:1751–1759
4. Khashan KS, Hassan AI, Addie AJ (2016) Characterization of CuO thin films deposition on porous silicon by spray pyrolysis. *Surf Rev Lett* 23(05):1650044
5. Krishnakumar T, Jayaprakash R, Prakash T, Sathyaraj D, Donato N, Licocchia S, Latino M, Stassi A, Neri G (2011) CdO-based nanostructures as novel CO₂ gas sensors. *Nanotechnology* 22(32):325501
6. Hong C, Zhou Q, Lu Z, Umar A, Kumar R, Wei Z, Wu X, Xu L, Kim SH (2017) Ag-doped ZnO nanoellipsoids based highly sensitive gas sensor. *Mater Express* 7(5):380–388
7. Tsai YT, Chang SJ, Ji LW, Hsiao YJ, Tang IT, Lu HY, Chu YL (2018) High sensitivity of NO gas sensors based on novel Ag-doped ZnO nanoflowers enhanced with a UV light-emitting diode. *ACS Omega* 3(10):13798–13807
8. Navale S, Shahbaz M, Mirzaei A, Kim SS, Kim HW (2021) Effect of Ag addition on the gas-sensing properties of nanostructured resistive-based gas sensors: an overview. *Sensors* 21(19):6454
9. Hussain ZT, Khashan KS, Mahdi RO (2021) Characterization of cadmium oxide nanoparticles prepared through Nd: YAG laser ablation process. *Mater Today Proc* 42:2645–2648
10. Şahin B (2013) Physical properties of nanostructured CdO films from alkaline baths containing saccharin as additive. *Sci World J* 2013
11. Mohanraj K, Balasubramanian D, Chandrasekaran J, Bose AC (2018) Synthesis and characterizations of Ag-doped CdO nanoparticles for PN junction diode application. *Mater Sci Semicond Process* 79:74–91
12. Vadgama VS, Vyas RP, Jogiya BV, Joshi MJ (2017) Synthesis and characterization of CdO nano particles by the sol-gel method. In *AIP Conference Proceedings* (Vol. 1837, No. 1, p. 040016). AIP Publishing LLC
13. Abbas S, Basma H, Al Boukhari J, Awad R (2021) Characterization of CdO nanoparticles prepared by co-precipitation method under different pH and calcination temperatures. *Appl Phys A* 127(7):1–17
14. Dakhel AA (2018) Electronic transport and optical properties of nano-structured Pt-doped CdO films: evaluate the effect of treatment in hydrogen gas. *J Mater Sci Mater Electron* 29(5):3584–3591
15. Alharbi SR, Qasrawi AF (2021) Effects of Au nanoslabs on the performance of CdO thin films designed for optoelectronic applications. *Phys E* 125:114386
16. Saimon JA, Madhat SN, Khashan KS, Hassan AI (2018) Characterization of CdZnO/Si heterojunction photodiode prepared by pulsed laser deposition. *Int J Mod Phys B* 32(31):1850341
17. Maity R, Chattopadhyay KK (2006) Synthesis and characterization of aluminum-doped CdO thin films by sol–gel process. *Sol Energy Mater Sol Cells* 90(5):597–606
18. Kose S, Atay F, Bilgin V, Akyuz I (2009) In doped CdO films: electrical, optical, structural and surface properties. *Int J Hydrogen Energy* 34(12):5260–5266
19. Gülen Y, Şahin B, Bayansal F, Cetinkara HA (2014) Solution-phase synthesis of un-doped and Pb doped CdO films. *Superlattices Microstruct* 68:48–55
20. Güney H, İskenderoğlu D (2021) CdO: Ag semiconductor nanowires grown by spray method. *J Alloy Compd* 865:158924
21. Salem A (2014) Silver-doped cadmium oxide nanoparticles: synthesis, structural and optical properties. *Eur Phys J Plus* 129(12):1–12
22. Yüksel M, Şahin B, Bayansal F (2016) Nano structured CdO films grown by the SILAR method: influence of silver-doping on the morphological, structural and optical properties. *Ceram Int* 42(5):6010–6014
23. Khashan KS, Sulaiman GM, Mahdi R (2018) The effect of laser energy on the properties of carbon nanotube—iron oxide nanoparticles composite prepared via pulsed laser ablation in liquid. *Mater Res Express* 5(10):105004
24. Khashan KS, Mahdi F (2017) Synthesis of ZnO: Mg nanocomposite by pulsed laser ablation in liquid. *Surf Rev Lett* 24(07):1750101
25. Khashan KS, Hadi A, Mahdi M, Hamid MK (2019) Nanosecond pulse laser preparation of InZnO (IZO) nanoparticles NPs for high-performance photodetector. *Appl Phys A* 125(1):1–7
26. Khashan KS, Abbas SF (2016) Characterization of InN nanoparticles prepared by laser as photodetector. *Int J Mod Phys B* 30(14):1650080

27. Khashan KS, Abbas SF (2019) Indium nitride nanoparticles prepared by laser ablation in liquid. *Int J Nanosci* 18(02):1850021
28. Khashan KS, Ismail RA, Mahdi RO (2018) Synthesis of SiC nanoparticles by SHG 532 nm Nd: YAG laser ablation of silicon in ethanol. *Appl Phys A* 124(6):1–11
29. Kaviyarasu K, Manikandan E, Paulraj P, Mohamed SB, Kennedy J (2014) One dimensional well-aligned CdO nanocrystal by solvothermal method. *J Alloy Compd* 593:67–70
30. Khan ZR, Alshammari AS, Shkir M, Bouzidi M, Mohamed M, Kumar M, Sonker RK (2022) Effect of Ag doping on structural, morphological and optical properties of CdO nanostructured thin films. *Phys B Condens Matter* 632:413762
31. Li Y, Ling H, Gao L, Song YL, Tian ML, Zhou FQ (2015) Synthesis, structure and optical properties of CdO nanocrystals directly grown on Cd foil. *Chin Phys Lett* 32(10):107802
32. Ansari SG, Borojerdian P, Sainkar SR, Karekar RN, Aiyer RC, Kulkarni SK (1997) Grain size effects on H₂ gas sensitivity of thick film resistor using SnO₂ nanoparticles. *Thin Solid Films* 295(1–2):271–276
33. Singh SK, Dutta D, Dhar A, Das S, Paul MC, Gangopadhyay TK (2019) Detection of ammonia gas molecules in aqueous medium by using nanostructured Ag-doped ZnO thin layer deposited on modified clad optical fiber. *Phys Status Solidi A* 216(16):1900141
34. Singh SK, Samanta UK, Dhar A, Chandra Paul M (2021) Structural, morphological, and optical properties of Ag-doped TiO₂ thin-film over fiber optic substrate for sensing applications. *Phys Status Solidi A* 218(22):2100447
35. Yousif AA, Hasan MH (2015) Gas sensitivity and morphologically characterized of nanostructure CdO doped In₂O₃ films deposited by pulsed laser deposition. *J Biosens Bioelectron* 6(4):4–10
36. Soltabayev B, Yıldırım MA, Ateş A, Acar S (2019) The effect of indium doping concentration on structural, morphological and gas sensing properties of IZO thin films deposited SILAR method. *Mater Sci Semicond Process* 101:28–36
37. Nam B, Ko TK, Hyun SK, Lee C (2020) Sensitivities of a 6: 4 (by molar ratio) ZnO/WO₃ composite nanoparticle sensor to reducing and oxidizing gases. *Appl Surf Sci* 504:144104
38. Xing X, Yang Y, Yan Z, Hu Y, Zou T, Wang Z, Wang Y (2019) CdO-Ag-ZnO nanocomposites with hierarchically porous structure for effective VOCs gas-sensing properties. *Ceram Int* 45(4):4322–4334
39. Wang CN, Li YL, Gong FL, Zhang YH, Fang SM, Zhang HL (2020) Advances in doped ZnO nanostructures for gas sensor. *Chem Rec* 20(12):1553–1567

Publisher's Note Springer Nature remains neutral with regard to jurisdictional claims in published maps and institutional affiliations.

Springer Nature or its licensor (e.g. a society or other partner) holds exclusive rights to this article under a publishing agreement with the author(s) or other rightsholder(s); author self-archiving of the accepted manuscript version of this article is solely governed by the terms of such publishing agreement and applicable law.